Available online at www.sciencedirect.com
ScienceDirect
Journal of the European Ceramic Society 28 (2008) 259–265
www.elsevier.com/locate/jeurceramsoc

# Hot corrosion of γ-$Y_2Si_2O_7$ in strongly basic $Na_2CO_3$ molten salt environment

Ziqi Sun [a,b], Meishuan Li [a], Zhongping Li [c], Yanchun Zhou [a,*]

[a] *Shenyang National Laboratory for Materials Science, Institute of Metal Research, Chinese Academy of Sciences, 72 Wenhua Road, Shenyang 110016, China*
[b] *Graduate School of Chinese Academy of Sciences, Beijing 100039, China*
[c] *National Key Laboratory of Advanced Functional Composite Materials, Beijing 100076, China*

Received 24 January 2007; received in revised form 23 April 2007; accepted 13 May 2007
Available online 26 July 2007

**Abstract**

γ-$Y_2Si_2O_7$ is a promising candidate both for high temperature structural applications and as thermal barrier coatings due to its unique combination of properties, such as high melting point, good machinability, high thermal stability, low linear thermal expansion coefficient ($3.9 \times 10^{-6}\,K^{-1}$, 25–1400 °C) and low thermal conductivity (<3 W/m K above 300 °C). In this work, the hot corrosion behavior of γ-$Y_2Si_2O_7$ in strongly basic $Na_2CO_3$ molten salt at 850–1000 °C for 20 h in flowing air was investigated. In the employed conditions, multi-layer corrosion scales with total thickness less than 90 μm were formed. At 850–900 °C, the outmost layer of the scale was composed of the reprecipitation of $Y_2O_3$, the bottom of a Si-rich $Na_2O{\cdot}xSiO_2$ ($x > 3.65$) melt layer, and the middle of a $NaYSiO_4$ layer. At 1000 °C, the corrosion products turned out to be a mixture of $NaY_9Si_6O_{26}$ and Si-rich $Na_2O{\cdot}xSiO_2$ ($x > 3.65$). In all cases, a thin layer of protective $SiO_2$ formed under the $Na_2O{\cdot}xSiO_2$ melt and protected the bulk material from further corrosion.


*Keywords:* $Y_2Si_2O_7$; Corrosion; Silicates; Structural applications; Engine components

## 1. Introduction

Ceramic materials exhibit numerous excellent properties, such as good thermal stability, wear and corrosion resistance, etc. Therefore, a great number of ceramics have been served in high temperature and extremely corrosive environments. Such kinds of applications include (a) refractories subjected to the action of alkali vapors or slag in glass furnaces, blast furnaces and stove construction, cement kiln linings, combustion chamber boilers and town gas installations; (b) advanced high temperature coal conversion and combustion, heat exchangers, and other energy systems. The great challenge to the reliability of structural ceramics in these environments is the requirement of good resistance to the attack of alkalis. However, many ceramics can be easily attacked by alkalis; thus, understanding of the attack mechanism and protection of ceramics from alkalis become an important subject.[1]

Silicon-based ceramics, such as $Si_3N_4$, SiC and fiber-reinforced SiC ceramic matrix composites (SiC/SiC CMCs), all exhibit superior high temperature strength and durability, which enable the revolutionized gas turbine engine technology.[2,3] In combustion system, various compounds such as $Na_2CO_3$ and $Na_2SO_4$ may be generated in addition to combustion gases.[4] In these alkali environments, corrosion of silicon-based ceramics is accelerated due to the fact that the protective $SiO_2$ thin film formed on the surface of silicon-based non-oxide ceramics would be dissolved in alkali molten salt.[1,5–12] This result is undesirable for high temperature engineering applications. In order to conquer this shortcoming, some silicates have been considered as protective coatings on SiC or $Si_3N_4$ ceramics. These silicates exhibit many attributes, like environmental stability, low coefficient of thermal expansion (CET), chemical stability and good adhesion with Si-based ceramics.[3] Recent investigations have also demonstrated that the oxides with a general formula of $A_2B_2O_7$, in particular the rare earth disilicates, have a

* Corresponding author at: High-Performance Ceramic Division, Shenyang National Laboratory for Materials Science, Institute of Metal Research, Chinese Academy of Sciences, 72 Wenhua Road, Shenyang 110016, China.
Tel.: +86 24 23971765; fax: +86 24 23891320.
*E-mail address:* yczhou@imr.ac.cn (Y. Zhou).

0955-2219/$ – see front matter © 2007 Elsevier Ltd. All rights reserved.
doi:10.1016/j.jeurceramsoc.2007.05.011

potential application as efficient environmental/thermal barrier coatings.[12]

Yttrium disilicate ($Y_2Si_2O_7$), one of the most refractory silicates with a melting point of 1775 °C, is a potential candidate material for high temperature structural applications.[13] When $Y_2O_3$ or $Y_2O_3 + SiO_2$ is used as the sintering aid for silicon nitride ($Si_3N_4$), $Y_2Si_2O_7$ forms as an intergranular phase and plays an important role in the sintering of $Si_3N_4$. If $Y_2Si_2O_7$ was used as a sintering aid of $Si_3N_4$ directly, it could provide the as-sintered $Si_3N_4$ with better high temperature properties.[14–16] Hence, the properties of $Y_2Si_2O_7$ have a strong influence on the performance of $Si_3N_4$. Moreover, yttrium silicate/disilicate has promising applications as oxidation protective coatings on SiC/C composites.[17–19]

In our previous work, pure γ-$Y_2Si_2O_7$ bulk material has been successfully prepared utilizing a pressureless sintering method at a relatively low temperature and for a short holding time using the powders synthesized by the solid/liquid reaction method with $LiYO_2$ additive.[20] γ-$Y_2Si_2O_7$ is a high temperature phase among the six polymorphs of yttrium disilicate (y, α, β, γ, δ, and properly z) and it is extremely stable in a wide temperature range. The thermal expansion of polycrystalline γ-$Y_2Si_2O_7$ linearly changes with temperature from 25 °C to 1400 °C and the linear thermal expansion coefficient is determined to be $3.9 \times 10^{-6}\,K^{-1}$, which is close to that of SiC or $Si_3N_4$.[21] We have also found that γ-$Y_2Si_2O_7$ has a low thermal conductivity (<3 W/m K above 300 °C). The superior thermal transport properties guarantee γ-$Y_2Si_2O_7$ to be a candidate as thermal barrier coatings. In addition, γ-$Y_2Si_2O_7$ is readily machinable and can be drilled easily by conventional cemented carbide tools.[22] The unique combination of the properties, such as machinability, thermal stability, low thermal expansion coefficient, and low thermal conductivity enable γ-$Y_2Si_2O_7$ a promising candidate either in high temperature structural applications or as environmental/thermal barrier coatings. Therefore, a comprehensive understanding of the hot corrosion behavior of yttrium disilicate is necessary.

In this work, we studied the hot corrosion of γ-$Y_2Si_2O_7$ in $Na_2CO_3$ molten salt at various temperatures (850–1000 °C). Compared with extensively studied $Na_2SO_4$, $Na_2CO_3$ decomposes more readily and it is usually used to study the corrosion under a strongly basic condition.

$$Na_2CO_3(l) = Na_2O(s) + CO_2(g) \quad (1)$$

Almost all silicon-based ceramics are corroded severely in $Na_2CO_3$ molten salt condition due to the dissolution of passive $SiO_2$ thin film in strongly basic molten salt.[5,7–10,23,24] For example, the hot corrosion study of $Si_3N_4$ in $Na_2CO_3$ molten salt showed that a preferential attack of the grain boundary occurred in $Y_2O_3$-doped samples.[5,10,24] For other silicon-based ceramics, such as SiC, a rapid alkali-assisted oxidation was observed in $Na_2CO_3$ molten salt.[7–10,23]

This paper aims at determining the hot corrosion mechanism of γ-$Y_2Si_2O_7$ in strongly basic molten salt environment at various temperatures. The result of this study will be helpful for the materials selection in high temperature and harsh condition applications, or for choosing the candidate of environmental/thermal barrier coatings.

## 2. Experimental procedure

### 2.1. Specimen preparation

Single-phase γ-$Y_2Si_2O_7$ was pressurelessly sintered according to the procedure described in our previous work.[20] Briefly, γ-$Y_2Si_2O_7$ powders were synthesized at 1400 °C for 4 h using $SiO_2$ and $Y_2O_3$ as starting materials. And then, the bulk material was obtained by pressureless sintering the synthesized powders at 1200 °C for 80 min in air. The final density of the samples used in this work was 3.80 g/cm$^3$ (94% of the theory density). SEM observation showed that a trace of amorphous $SiO_2$ presented as a secondary phase in grain boundaries.

Specimens for hot corrosion tests were cut to 8 mm × 6.5 mm × 1.4 mm using a diamond wafer. The as-cut specimens were ground on 1500 grid SiC paper and ultrasonically cleaned in acetone and then dried. To increase the wettability between the substrate and the salt coating, no polish was performed. The specimens were cleaned in a sequence of distilled water, acetone and alcohol, thereafter airbrushed with a saturated solution of $Na_2CO_3$ on a 250 °C hot plate. The amount of the salt was controlled to be $4.5 \pm 0.25$ mg/cm$^2$.

### 2.2. Specimen characterization

Hot corrosion experiments were carried out at 850 °C, 900 °C and 1000 °C. Mass changes were monitored by a Setsys 16/18 thermogravimetric analyzer with an accuracy of $\pm 4 \times 10^{-7}$ g (TGA; Setaram, Caluire, France), which was coupled with a mass spectrometer (MS; Ominstar, Asslar, Germany) to analyze the gas evolution during hot corrosion. The salt-coated specimens were put in a platinum basket which was suspended in TGA and the specimens were heated to the test temperatures at a rate of 40 °C/min. Duplicate runs were carried out to check the reproduction of tests. After the TGA tests, the characterizations of the corroded samples were performed in both the as-tested and the hot-distilled-water washed conditions.

The phase compositions of the as-corroded and washed specimens were identified by a step-scanning X-ray diffractometer with Cu Kα radiation (XRD; Rigaku D/max-2400, Tokyo, Japan). The surfaces and cross-sectional morphologies were observed by a scanning electron microscope (SEM; LEO SUPERA 35, Oberkochen, Germany) equipped with an energy-dispersive spectroscopy. Cross-sections were prepared by sputter plating ~1 μm of copper on the corroded samples, mounting them in epoxy, and polishing to 2000 grid SiC paper. The polished cross-sections were also examined with a scanning electron microscope and electron microprobe (EMPA1610, Shimadzu, Japan). For the EMPA measurements, $NaAlSiO_4$ was used as the standard reference of Si, Na and O, and yttrium metal as the standard of Y.

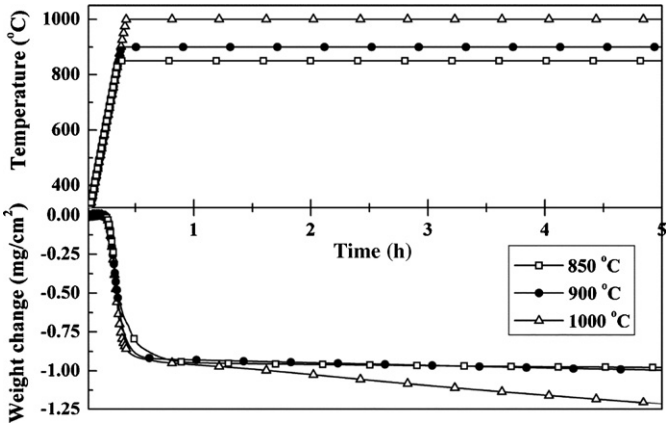


Fig. 1. Weight changes of γ-$Y_2Si_2O_7$ *vs.* time curves at different hot corrosion temperatures.

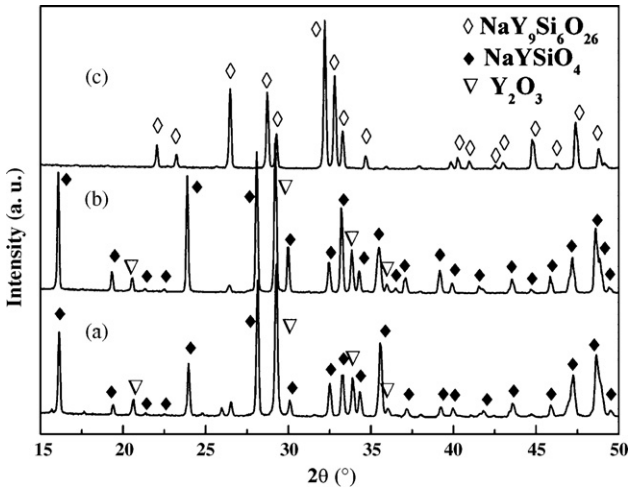


Fig. 2. XRD patterns detected from the γ-$Y_2Si_2O_7$ surface after hot corrosion tests at various temperatures: (a) 850 °C, (b) 900 °C, (c) 1000 °C.

## 3. Results

The plot of weight changes per unit area versus time at different temperatures for $Na_2CO_3$-coated γ-$Y_2Si_2O_7$ exposed in air is presented in Fig. 1. The curves only recorded the variations within the first 5 h because of a similar tendency thereafter. Combined with the results of mass spectrometer, the major weight loss at the initial stage was caused by the decomposition of $Na_2CO_3$ into $Na_2O$ and $CO_2$ above 550 °C. This decomposition reaction proceeded rapidly and completed within 1 h, after that, the evolution of $CO_2$ gas could not be detected by mass spectrometer any more. At the isothermal stage, a linear evaporation of $Na_2O$ was observed at all test temperatures and the linear evaporation rate constants are listed in Table 1. At 850 °C, the evaporation of $Na_2O$ was small and the linear rate constant was only $3.3 \times 10^{-3}$ mg/(cm$^2$ h). While at 1000 °C, the evaporation of $Na_2O$ increased obviously and the linear rate constant reached $4.8 \times 10^{-2}$ mg/(cm$^2$ h). The reliability values, *R*, as presented in Table 1, which indicate that the linear fits of evaporation of $Na_2O$ from the weight loss curves in isothermal stage in Fig. 1 were perfect.

After removing the residual salt, corrosion products were determined by XRD and the diffraction patterns are displayed in Fig. 2. For the samples corroded at 850 °C and 900 °C, the dominant crystalline phases were $NaYSiO_4$ and $Y_2O_3$. When corroded at 1000 °C, however, different products were detected. Two possible products, $Y_{4.67}(SiO_4)_3O$ and $NaY_9Si_6O_{26}$, fit the XRD peaks well. Assisted by the result of EDS spectra on the corrosion surface, $NaY_9Si_6O_{26}$ was determined to be the major product.

Table 1
Linear evaporation rate constants of $Na_2O$ molten salt at various temperatures

| Temperature (°C) | Linear evaporation rate constants (mg/cm$^2$ h) | *R* |
|---|---|---|
| 850 | $3.3 \times 10^{-3}$ | 0.994 |
| 900 | $1.3 \times 10^{-2}$ | 0.997 |
| 1000 | $4.8 \times 10^{-2}$ | 0.998 |

Surface morphologies and cross-sections from the same piece of specimen after $Na_2CO_3$ hot corrosion are displayed in Fig. 3. Before observation, all samples were treated in boiling distilled water for 30 min to remove the residual salt. At 850 °C (Fig. 3a) and 900 °C (Fig. 3c), many white spots appeared on the corroded surface. EDS analysis confirmed that the white spots were rich in yttrium (Y: 37.83 at.%, Si: 6.9 at.%, O: the rest) but no sodium was detected. Combined with the XRD pattern in Fig. 2, these white spots were assumed to be $Y_2O_3$. Besides the white spots, a number of cracks and pores were also present on the surface. The cracks might be caused by the thermal stress resulted from the mismatch of thermal expansion coefficients between corrosion products and the substrate. And the pores might be the channels for the release of $CO_2$ gas. The cross-section images of the 850 °C (Fig. 3b) and 900 °C (Fig. 3d) samples presented a multi-layer corrosion scales: the top of the corrosion scale was a white $Y_2O_3$ layer, the bottom was a dark layer of silicon-rich product, and the middle was a gray $NaYSiO_4$ layer, according to the XRD and EMPA results (Table 2). The surface of the 1000 °C corroded specimen shows a "pin-like" morphology (Fig. 3e). The corrosion product can be determined to be $NaY_9Si_6O_{26}$ combining the results of XRD and EMPA. It is noted from the SEM image of the cross-section (Fig. 3f) that the pin-like yttrium-rich $NaY_9Si_6O_{26}$ was isolated from the molten salt and left behind dark silicon-rich product. The summary of scale thickness, EMPA elemental quantitative analysis and phase identification of the corrosion scales are all listed in Table 2.

Fig. 4 shows the EMPA X-ray elemental distribution maps collected from the polished cross-section of 900 °C corroded specimen. The corrosive Na species was detected across the whole corrosion scale and at the grain boundary of the substrate as well, as illustrated in the map for Na element. This implies that $Na_2O$ had penetrated into the bulk $Y_2Si_2O_7$ body. The outmost of the corrosion scale should be a layer of $Y_2O_3$ because this region was rich in Y but deficient in Si and Na elements. At the bottom, however, a small stripe, which was rich in Na, Si and superposed with the Y-poor zone, was $Na_2O{\cdot}xSiO_2$. The elemental quantitative results of EMPA show that the value of

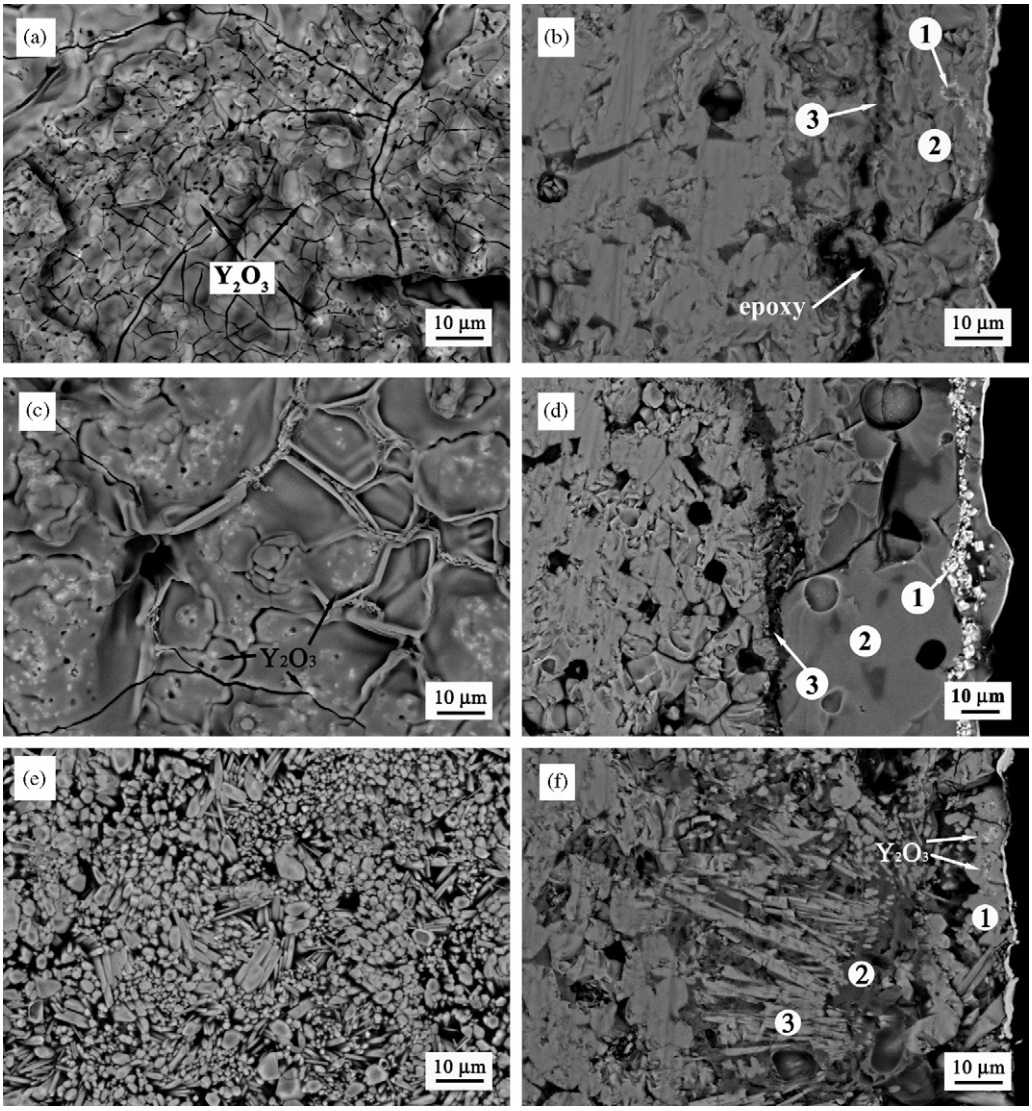


Fig. 3. SEM micrographs of the distilled-water washed surfaces and cross-sections of hot corrosion specimens from 850–1000 °C for 20 h: (a and b) for 850 °C, (c and d) for 900 °C, (e and f) for 1000 °C.

$x$ for $Na_2O{\cdot}xSiO_2$ was higher than 3.65 (Table 2). Moreover, a thin layer of $SiO_2$ existed under the $Na_2O{\cdot}xSiO_2$ melt since the Si-rich region was slightly thicker than that of Na-rich region for this stripe from Na-map and Si-map.

## 4. Discussion

Fig. 1 is the mass variation of $Na_2CO_3$-coated γ-$Y_2Si_2O_7$ with time at different temperatures. At the initial reaction stage,

Table 2
Summary of experimental conditions, corrosion thicknesses, chemical contents and identified phases at the corresponding positions in Fig. 3

| Temperature (°C) | Corrosion scale thickness (μm) | Position number | WDS (at.%) | | | | Phases identification |
|---|---|---|---|---|---|---|---|
| | | | Na | Y | Si | O | |
| 850 | ~40 | 1 | – | 37.83 | 6.90 | 55.27 | $Y_2O_3$ |
| | | 2 | 10.09 | 17.18 | 17.44 | 55.29 | $NaYSiO_4$ |
| | | 3 | 13.58 | 8.89 | 20.37 | 57.16 | Si-rich melt |
| 900 | ~60 | 1 | – | 41.51 | – | 58.49 | $Y_2O_3$ |
| | | 2 | 11.44 | 18.23 | 18.20 | 52.13 | $NaYSiO_4$ |
| | | 3 | 10.65 | 7.83 | 25.58 | 55.94 | Si-rich melt |
| 1000 | ~90 | 1 | 2.41 | 26.26 | 17.20 | 54.13 | $NaY_9Si_6O_{26}$ |
| | | 2 | 11.32 | 8.48 | 25.18 | 55.02 | Si-rich melt |
| | | 3 | 2.69 | 25.77 | 17.86 | 53.68 | $NaY_9Si_6O_{26}$ |

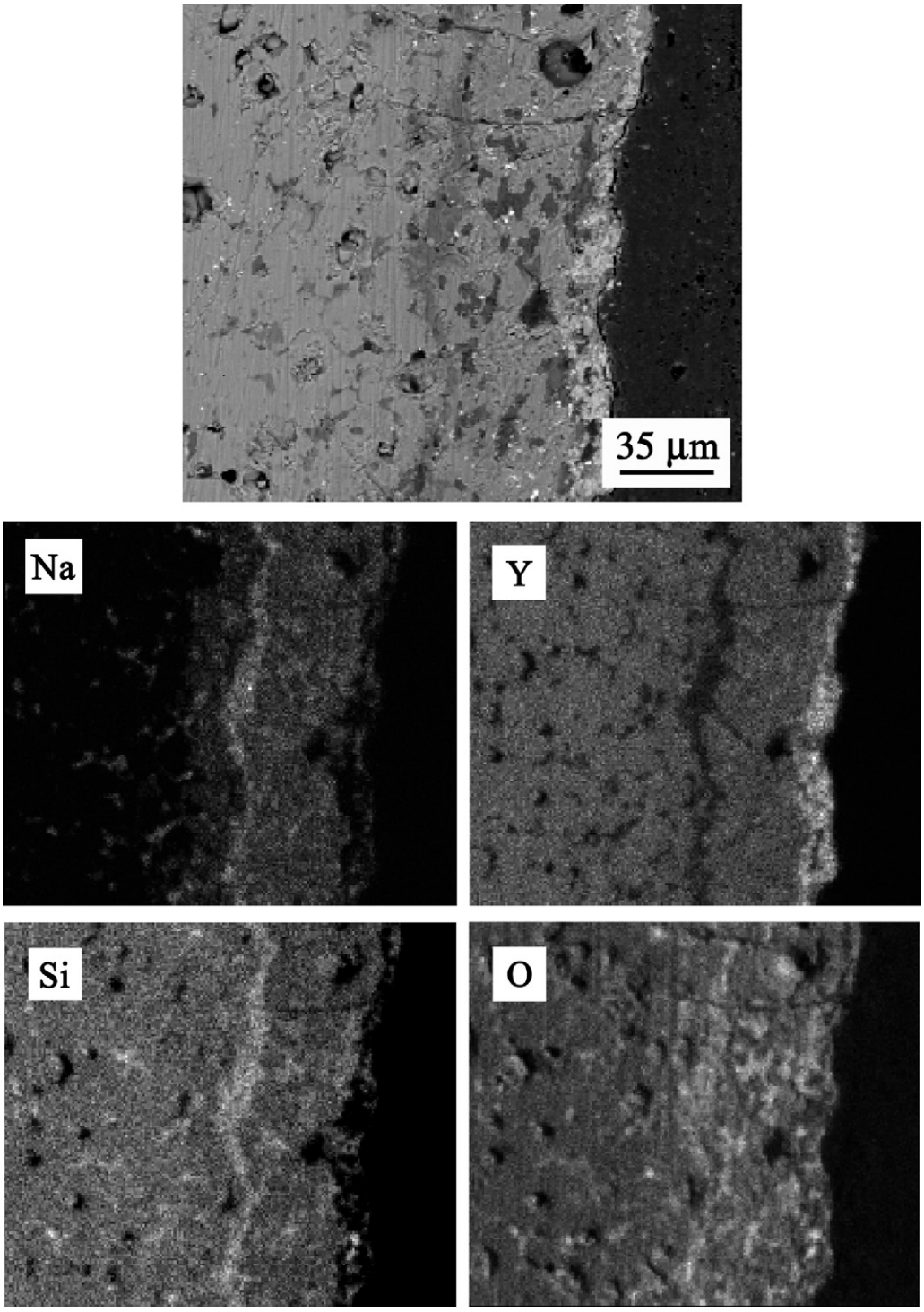


Fig. 4. SEM cross-section micrograph and the corresponding elemental distribution maps of the 900 °C hot corroded specimen.

the rapid weight change was caused by the release of $CO_2$ gas which came from the decomposition of $Na_2CO_3$. While at the isothermal corrosion stage, the slight weight loss was aroused by the linear evaporation of $Na_2O$. Because $Na_2CO_3$ was totally transformed to $Na_2O$ and $CO_2$, the hot corrosion of $\gamma$-$Y_2Si_2O_7$ was only induced by the strongly basic $Na_2O$ molten salt. Since both the substrate and the salt were oxides, the hot corrosion processes in this experiment were oxygen partial pressure independent. Therefore, we can speculate on the corrosion paths as follows.

In the as-received samples, a grain boundary phase $SiO_2$ was observed. Thus, $Na_2O$ melt attacked the grain boundaries first and then penetrated into the inner part of the sample. The reaction of $Na_2O$ with grain boundary phase $SiO_2$ is quite favorable[5,6]:

$$Na_2O(l) + xSiO_2(s) = Na_2O{\cdot}xSiO_2(l) \quad (2)$$

Thereafter, the melt surrounded the grains or collected grains and then reacted with $Y_2Si_2O_7$ (to simplify the reaction equation, we take $x = 1$ for $Na_2O{\cdot}xSiO_2$):

$$3Na_2O(l) + Y_2Si_2O_7(s) = 2NaYO_2(l) + 2Na_2O{\cdot}SiO_2(l)$$

or

$$3O^{2-} + Y_2Si_2O_7 = 2YO_2^- + 2SiO_3^{2-} \quad (3)$$

During the hot corrosion process, $Y_2Si_2O_7$ reacted with $Na_2O$ and $YO_2^-$ and $SiO_3^{2-}$ ions formed at the substrate/salt interface. Subsequently, the $YO_2^-$ ions would diffuse outwards due to the basicity (or $Na_2O$) gradient between the oxide/salt interface and salt/gas interface.[25,26] The salt/gas interface had a relatively lower $Na_2O$ (or $O^{2-}$) concentration than the inner part because of the evaporation of $Na_2O$ and the flowing air atmosphere. According to Rapp and Goto's proposition,[25] a "negative solubility gradient" for oxides would exist in the molten salt film along with the basicity (or $Na_2O$) gradient. The "negative solubility gradient" favors dissolution of oxide at the substrate/salt interface and reprecipitation of non-protective loose particles at the salt/gas interface. Deanhardt and Stern measured the solubility of $Y_2O_3$ in sodium molten salt.[27] $YO_2^-$ formed at the substrate/salt interface, which had a high $Na_2O$ activity and high $YO_2^-$ solubility, would diffuse to the salt/gas interface and reprecipitate as yttria.

$$2YO_2^- = Y_2O_3 + O^{2-} \quad (4)$$

On the other hand, $SiO_3^{2-}$ could not reprecipitate from the melt since the solubility of $SiO_2$ was independent of $Na_2O$ activity under basic conditions.[28] Thus $Na_2O{\cdot}xSiO_2$ was left and became rich in the oxide/salt region.

In the 850 °C and 900 °C corroded specimens, as mentioned above, $Y_2O_3$ was observed on the corrosion surface (as the white spots on the surfaces in Fig. 3a and c). And a continuous loose $Y_2O_3$ layer presented at the 900 °C cross-section (Fig. 3d). The yttria was the resulting product of dissolution and then reprecipitation of $YO_2^-$. At the bottom of corrosion scales for all corroded specimens, a dark region rich in Na and Si was shown in Fig. 3b, d and f. Though a little yttrium element was detected, this Si-rich product should be $Na_2O{\cdot}xSiO_2$ as indicated by the EMPA results in Table 2. The increasing of silicon content in this compound corresponded to a shift toward the silica-rich phase according to the $Na_2O$–$SiO_2$ phase diagram.[29] It was reported that once the liquid $Na_2O{\cdot}xSiO_2$ ($x = 3.65$) was approached, a silica layer would form beneath the silicate melt due to the decomposition of sodium silicates and eventually seal off the bulk material from further corrosion.[5,7,29] In this work, the molar ratio of $SiO_2$ to $Na_2O$ exceeded 3.65 based on the EMPA analysis. Therefore, a silica layer should form under the Si-rich sodium silicate melt. From the Na and Si maps in Fig. 4 we observed that a layer of $SiO_2$ appeared under the silicate melt. This thin layer of $SiO_2$ isolated the substrate from corrosive melt and provided protection to the material.

At high temperatures, the well mixed $YO_2^-$ and $SiO_3^{2-}$ tended to react with $Na^+$ and formed a new compound. At 850 °C and 900 °C, the product was $NaYSiO_4$ according to the XRD analysis.

$$Na^+ + YO_2^- + SiO_3^{2-} = NaYSiO_4(s) + O^{2-}$$

or

$$NaYO_2(l) + Na_2O{\cdot}SiO_2(l) = NaYSiO_4(s) + Na_2O(l) \quad (5)$$

When the corrosion temperature increased to 1000 °C, the corrosion products were different from those corroded at 850 °C and 900 °C as shown in the XRD patterns. At the initial stage of corrosion, reactions (2) and (3) took place and $Y_2Si_2O_7$ dissolved into molten salt in the form of $YO_2^-$ and $SiO_3^{2-}$. And $YO_2^-$ ions would also move to the outmost of the scale to form $Y_2O_3$. However, at such high temperature, $Y_2O_3$ was more likely to react with Si-rich melt and led to the formation of $NaY_9Si_6O_{26}$:

$$9Y_2O_3(s) + 2Na^+ + 12SiO_3^{2-} = 2NaY_9Si_6O_{26}(s) + 11O^{2-} \quad (6)$$

Some residual $Y_2O_3$ particles were still observed at the top of corrosion scale (corresponding to the white spots at the top of corrosion scale in Fig. 3f). Moreover, the $YO_2^-$ ion would also react with Si-rich melt to form $NaY_9Si_6O_{26}$ during the transportation process.

$$Na^+ + 9YO_2^- + 6SiO_3^{2-} = NaY_9Si_6O_{26}(s) + 10O^{2-} \quad (7)$$

As a result, the pin-like $NaY_9Si_6O_{26}$ crystal was precipitated from the melt as the major corrosion product at 1000 °C and the Si-rich phase was left behind (Fig. 3f).

In general, γ-$Y_2Si_2O_7$ can be corroded under the extremely strongly basic $Na_2CO_3$ molten salt. However, the thicknesses of the corrosion scales were less than 90 μm after 20 h exposure. This was attributed to the formation of a thin layer of protective $SiO_2$ formed under the $Na_2O{\cdot}xSiO_2$ melt scale, which protected the bulk material from further corrosion.

## 5. Conclusions

We investigated the hot corrosion behavior of $Na_2CO_3$-coated γ-$Y_2Si_2O_7$ exposed in flowing air at 850–1000 °C for 20 h. Multi-layer corrosion scales less than 90 μm were formed on the specimens. At 850–900 °C, the outermost of the corrosion scales was a loose film of $Y_2O_3$ particles due to the "negative solubility gradient". The bottom was a Y-deficient layer since Y element moved to the top of the scale in the form of $YO_2^-$. The middle layer was a layer of Si-rich melt corresponding to $Na_2O{\cdot}xSiO_2$ ($x > 3.65$). In the case of 1000 °C, the main corrosion product was pin-like $NaY_9Si_6O_{26}$ interlaced with sodium silicate ($Na_2O{\cdot}xSiO_2$ ($x > 3.65$)). The ($Na_2O{\cdot}xSiO_2$ ($x > 3.65$)) melt in all specimens provided protection against a further corrosion due to the fact that a silica layer could grow from this silicon-rich melt and seal off the bulk material. During the hot corrosion processes, a linear evaporation of $Na_2O$ molten salt was observed and the linear evaporation rate constants were obtained by fitting the weight loss curves at the holding stage.

## Acknowledgments

This work was supported by the National Outstanding Young Scientist Foundation for Y.C. Zhou under grant no. 59925208, Natural Sciences Foundation of China under grant nos. 50232040, 50302011, 90403027, and '863' project.

## References

1. Gogotsi, Y. G. and Lavrenko, V. A., *Corrosion of high-performance ceramics*. Springer-Verlag, Berlin, 1992, pp. 1–2.
2. Ziegler, G., Neinrich, J. and Wötting, G., Review, relationships between processing, microstructure and properties of dense and reaction-bonded silicon nitride. *J. Mater. Sci.*, 1987, **22**, 3041–3086.
3. Lee, K. N., Fox, D. S. and Bansal, N. P., Rare earth silicate environmental barrier coatings for SiC/SiC composites and $Si_3N_4$ ceramics. *J. Eur. Ceram. Soc.*, 2005, **25**, 1705–1715.
4. Birks, N. and Meier, G. H., *Introduction to high-temperature oxidation of metals*. Edward Arnold, London, UK, 1983 [Chapter 8].
5. Fox, D. and Jacobson, N. S., Molten-salt corrosion of silicon nitride: 1. Sodium carbonate. *J. Am. Ceram. Soc.*, 1988, **71**, 128–138.
6. Jacobson, N. S. and Fox, D., Molten-salt corrosion of silicon nitride: 2. Sodium sulfate. *J. Am. Ceram. Soc.*, 1988, **71**, 139–148.
7. Jacobson, N. S., Kinetics and mechanism of corrosion SiC by molten salts. *J. Am. Ceram. Soc.*, 1986, **69**, 74–82.
8. Li, T. K., Hirschfeld, D. A. and Brown, J. J., Alkali corrosion resistant coatings for $Si_3N_4$ ceramics. *J. Mater. Sci.*, 1997, **32**, 4455–4461.
9. McKee, D. W. and Chatterji, D., Corrosion of silicon carbide in gases and alkaline melts. *J. Am. Ceram. Soc.*, 1976, **59**, 441–444.
10. Pickrell, G. R., Sun, T. and Brown Jr., J. J., High temperature alkali corrosion of SiC and $Si_3N_4$. *Fuel Proc. Technol.*, 1995, **44**, 213–236.
11. Song, D. Y., Kitaoka, S. and Kawamoto, H., Hot corrosion of chemical vapor deposited SiC and $Si_3N_4$ in molten $Na_2SO_4$ salt. *J. Mater. Sci.*, 1998, **33**, 1031–1036.
12. Clarke, D. R. and Phillpot, S. R., Thermal barrier coating materials. *Materialstoday*, 2005, **8**, 22–29.
13. Levin, E. M., Robbins, C. R. and McMurdie, H. F., *Phase diagrams for ceramists—1969 supplement*. The American Ceramic Society Inc., Columbus, OH, 1969, p. 76 [Fig. 2388].
14. Hong, Z. L., Yoshida, H., Ikuhara, Y., Nishimura, T. and Mitomo, M., The effect of additives on sintering behavior and strength retention in silicon nitride with RE-disilicate. *J. Eur. Ceram. Soc.*, 2002, **22**, 527–534.
15. Lee, W. E., Drummond, C. H., Hilmas, G. E. and Kumar, S., Microstructural evolution in near-eutectic yttrium silicate compositions fabricated from a bulk melt and as an intergranular phase in silicon-nitride. *J. Am. Ceram. Soc.*, 1990, **73**, 3575–3579.
16. Choi, H. J., Lee, J. G. and Kim, Y. W., High temperature strength and oxidation behavior of hot pressed silicon nitride–disilicate ceramics. *J. Mater. Sci.*, 1997, **32**, 1937–1942.
17. Kondo, M., Ogura, Y. and Morimoto, T., Chemical stability between $Y_2SiO_5$ and SiC in an oxidation protection system for carbon/carbon composites. *Mater. Trans. JIM*, 1998, **39**, 1146–1151.
18. Aparicio, M. and Durán, A., Yttrium silicate coatings for oxidation protection of carbon–silicon carbide composites. *J. Am. Ceram. Soc.*, 2000, **83**, 1351–1355.
19. Seifert, H. J., Wagner, S., Fabrichnaya, O., Lukas, H. L. and Aldinger, F., Yttrium silicate coatings on chemical vapor deposition-SiC-protected C/C-SiC: thermodynamic assessment and high-temperature investigation. *J. Am. Ceram. Soc.*, 2005, **88**, 424–430.
20. Sun, Z. Q., Zhou, Y. C. and Li, M. S., Low temperature synthesis and sintering of $\gamma$-$Y_2Si_2O_7$. *J. Mater. Res.*, 2006, **21**, 1443–1450.
21. Sun, Z. Q., Zhou, Y. C. and Li, M. S, *Thermal properties and thermal shock resistance of $\gamma$-$Y_2Si_2O_7$*. Unpublished work.
22. Sun, Z. Q., Zhou, Y. C., Li, M. S. and Wang, J. Y., $\gamma$-$Y_2Si_2O_7$, a machinable silicate ceramics: mechanical properties and machinability. *J. Am. Ceram. Soc.*, 2007, **90**, 2535–2541.
23. Jacobson, N., Corrosion of silicon-based ceramics in combustion environments. *J. Am. Ceram. Soc.*, 1993, **76**, 3–28.
24. Mayer, M. and Riley, F. L., Sodium-assisted oxidation of reaction-bonded silicon nitride. *J. Mater. Sci.*, 1978, **13**, 1319–1328.
25. Rapp, R. A., Hot-corrosion of material: a fluxing mechanism? *Corros. Sci.*, 2002, **44**, 209–221.
26. Zhang, Y. S., Fluxing mechanism of hot corrosion and its limitation. *J. Chin. Soc. Corros. Protect.*, 1992, **12**, 1–10 [in Chinese].
27. Deanhardt, M. L. and Stern, K. H., Solubility of yttrium oxide in $Na_2SO_4$ and NaCl melts. *J. Electrochem. Soc.*, 1982, **129**, 2228–2232.
28. Shi, D. Z. and Rapp, R. A., The solubility of $SiO_2$ in fused $Na_2SO_4$ at 900 °C. *J. Electrochem. Soc.*, 1986, **133**, 849–850.
29. Kingery, W. D., Bowen, H. K. and Uhlmann, D. R., *Introduction to ceramics*. Wiley, New York, 1976, p. 359.